Synthesis and Characterization of $LiM_XFe_{1-X}PO_4$ (M = Cu, Sn; X = 0.02) Cathodes - A study on the Effect of Cation Substitution in $LiFePO_4$ Material

N. Jayaprakash, N. Kalaiselvi, P. Periasamy*

Central Electrochemical Research Institute, Karaikudi, India
*E-mail: kalakanth2@yahoo.com

An attempt has been made for the possible augmentation and exploration of partially substituted $LiFePO_4$ material as a positive electrode for lithium battery applications. In this regard, cationic substitution of Cu and Sn (2%) to the native $LiFePO_4$/C electro active material has been carried out via. ball milling, with a view to understand the effect of respective transition and non-transition metals upon $LiFePO_4$ individually. Uniformly distributed particles (SEM) of $LiM_XFe_{1-X}PO_4$/C (M= Cu, Sn) with phase pure nature (XRD) and finer crystallite size (<1μm) were obtained. Further, it is interesting to note that irrespective of the nature of the dopant metal, the simple route of ball milled $LiM_XFe_{1-X}PO_4$/C [M= Cu, Sn] cathodes endowed with improved conductivity and stable reversible capacity values (chare-discharge). In other words, the $LiCu_{0.02}Fe_{0.98}PO_4$/C cathode delivered a reversible capacity of ~105 mAh/g with an excellent capacity retention characteristic. On the other hand $LiSn_{0.02}Fe_{0.98}PO_4$/C cathodes exhibited an average specific capacity of ~100mAh/g with progressively enhanced efficiency values. Results of Fourier Transform Infra Red (FTIR) spectroscopy and Cyclic Voltammetric studies of $LiM_XFe_{1-X}PO_4$/C (M= Cu, Sn) composites are also appended and correlated suitably.

1. INTRODUCTION

Over the past few years, phosphate based olivine compounds have created substantial interest as battery active materials for rechargeable Li-ion batteries. Among the phospho-olivines of composition $LiMPO_4$ (M= Fe, Mn, Co & Ni) [1-3] that belong to the general class of polyanionic compounds, $LiFePO_4$ has gained paramount importance due to the easy availability of iron resources, eco benign nature and economically viable preparation methods. $LiFePO_4$, with a theoretical capacity of 170mAh/g, possesses very good electrochemical stability (even when it is used with common

organic electrolyte systems) [2-7], structural stability due to the strong covalent bonding of oxygen with P^{5+} to form the $(PO_4)^{3-}$ tetrahedral polyanion [1], and better thermal stability [8]. It is quite unfortunate that despite the mentioned advantages, certain critical and hampering issues such as poor rate capability and electrical conductivity [8] associated with the material makes it difficult to exploit the entire capacity of $LiFePO_4$ made available for rechargeable Li-ion battery applications.

Basically, investigations to improve the local cation structure and environment of $LiFePO_4$ material for conductivity enhancement [6,9-10] are well documented in terms of Mossbauer spectroscopy [6, 9], XAFS [10], magic angle spinning nuclear magnetic resonance techniques [11], FTIR and Raman studies [12]. On the other hand, efforts to improve the conductivity and electrochemical properties of $LiFePO_4$ by surface modification [13,14] or by acting on the phase composition through cationic substitution [15-17] are also reported.

Among the two methods of improving the electrochemical performance, the former has led to the formation of composite electrodes by the addition of conducting carbon [6], sucrose [13] etc., that has exhibited capacity values closer to 170mAh/g and with high rate capability [18]. However, it is necessary indeed to gain a complete understanding of effect of various parameters upon the performance of $LiFePO_4$ [19]. In this regard, literature is replete with the finding that factors such as phase purity of the active material [6], particle size [6], amount of added carbon [19], form/type of carbon added [20] and also the structure of the surface carbon [21], play significant role independently in determining the electrochemical performance of the battery, wherein the said factors are mainly synthetic route dependent. Further, it is quite interesting that Yamada etal., have recently demonstrated the possibility of realizing >95% of the theoretical capacity of $LiFePO_4$ by sintering the precursor materials at an optimum temperature, say 550° C, for the production of smaller particles with larger surface area available for the intercalation of Li-ions [6]. This in turn has directed a newer pathway of deployment of suitable synthesis method with optimized synthesis conditions to modify both the physical as well as electrochemical characteristics of $LiFePO_4$ material.

Therefore, it is quite obvious that not only the approach being adopted to improve the overall performance of $LiFePO_4$ electrode material gains importance, but also the selection and deployment of suitable synthesis methodology. Because, variety of synthesis methods that include mixing of precursor salt with a carbon gel, addition of sugar as carbon source [19], deployment of sol-gel [22], co-precipitation [23], emulsion drying [24], and microwave assisted synthesis methods [25] and the dispersal of carbon powders via. aqueous gelatins [20] are reported to have favorable impact over $LiFePO_4$ material.

Recently, our group has reported on the possible anode characteristics of the native and substituted $LiFePO_4/C$ composite for lithium battery applications [26,27]. As a sequel to that work and with a view to explore the maximum possible electrochemical performance of substituted $LiFePO_4$ derivatives, the present study has been designed. Towards this attempt, a transition (Cu) and a non-transition (Sn) metal have been chosen as dopants to be incorporated into the native $LiFePO_4/C$ matrix individually. Hence, a set of two compounds viz., $LiCu_{0.02}Fe_{0.98}PO_4/C$ and $LiSn_{0.02}Fe_{0.98}PO_4/C$ have been synthesized and characterized for the present study. Correlation of enhanced specific capacity values as a function of cation substitution and the chosen category synthesis methodology is also reported.

2. EXPERIMENTAL PART

2.1. Synthesis procedure

Stochiometric amount of Li_2CO_3, $Fe_2(C_2O_4)_3 \cdot 6H_2O$, $(NH_4)_2HPO_4$ and $CuCO_3 \cdot Cu(OH)_2$ or $SnCl_2$ (for substituted $LiFePO_4$) were mixed thoroughly with 10wt.% carbon and the mixture was ball milled for about 12h. to ensure intimate and homogeneous mixing. The added carbon is expected to form an uniform surface coating over the reactant mixture which may prevent the formation of unacceptable impurities, developed along with the required $LiFePO_4$ product at the final step. The ball milled fine powders of the precursor mixture was subjected initially to a lower calcination temperature of 450° C for 6 h. and subsequently to 750° C for 3 h. (rate of heating: 5° C per minute) with the deployment of periodical and intermittent grinding after every 3h. duration. The ultra fine powders obtained after the high temperature calcination of 750° C was collected from furnace and subjected further to systematic characterization studies.

2.2. Structural and morphological characterization

TG-DTA (thermogravimetry and differential thermal analysis) curves were obtained with a thermo balance model STA 409PC in the temperature range 0-600°C, using alumina crucibles with 31mg of samples, under dynamic nitrogen atmosphere at a heating rate of 20°C/min.   Phase characterization was done by powder X-ray diffraction technique on a Philips 1830 X- ray diffractometer using Ni filtered Cu Kα radiation (λ= 1.5406Å) in the 2θ range of 15-60 at a scan rate of 0.04°/s. Surface morphology of the particles was examined through SEM images obtained from Jeol S-3000 H Scanning Electron Microscope. Fourier Transform Infra Red spectroscopic study was performed on a Perkin-Elmer paragon-500 FTIR spectrophotometer using KBr pellets in the region of 400-1400 cm^{-1}. Electrochemical studies such as cyclic voltammetry and charge-discharge studies were carried out using Autolab electrochemical analyzer and MACCOR charge – discharge cycle life tester.

2.3. Electrochemical characterization

Cyclic Voltammetry and Charge discharge studies were carried out with crimp sealed 2016 coin cells. Lithium metal was used as the anode and 1M $LiPF_6$ in 1:1 v/v ethylene carbonate (EC) and dimethyl carbonate (DMC) as the electrolyte. The cathode was prepared by mixing 80% active material with 10% super-P black and 10% poly(vinylidene fluoride) (PVdF) binder in *N*-methyl-2-pyrrolidone (NMP), which was coated on an aluminum foil and dried at 120° C for 12 h. in an oven. The resulting slurry coated aluminum foil was roll-pressed and the electrode was punched out to the required dimension with a punching machine. 2016 coin cells were assembled in a glove box, crimp sealed and subjected further to CV and Charge-discharge studies.

3. RESULTS AND DISCUSSION

3.1. Thermal analysis- TG-DTA

Thermoanalytical curves obtained by the decomposition of $LiM_xFe_{1-x}PO_4$ (M= Cu, Sn; x = 0.02) precursor are shown in Figs.1a-b. The initial weight loss of about 2.7% observed in the range of 75–170°C may be assigned to the process of dehydration that results in the complete removal of water molecules [28] from the precursor mixture, along with the individual dehydration of $Fe_2(C_2O_4)_3.6\ H_2O$ salt. However, the dehydration of $Fe_2(C_2O_4)_3.6\ H_2O$ salt, which has a melting point of 100°C, is believed to be accompanied by the process of decarboxylation also to result in the formation of CO_2. Because, thermal decomposition of Fe(II) oxalate in N_2 atm. can proceed through two different paths [29]:
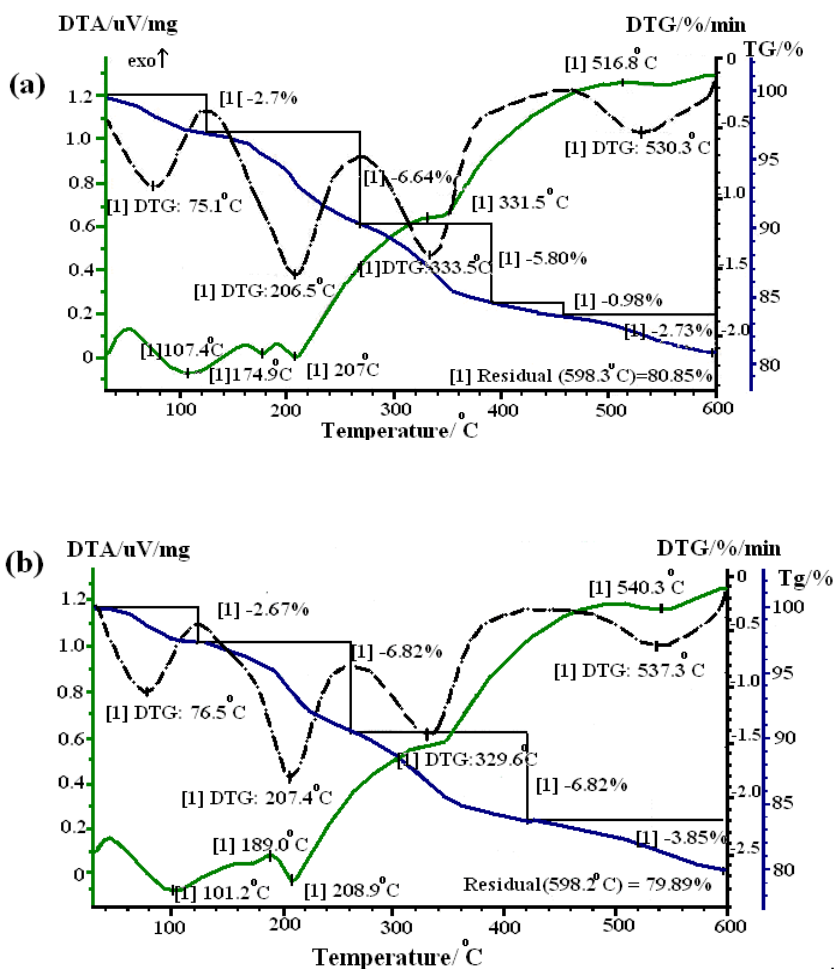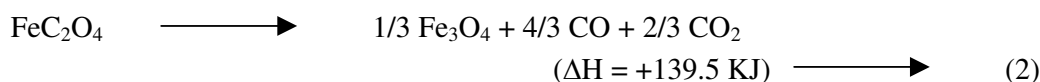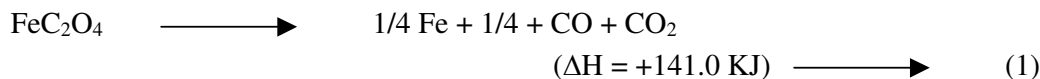
$$FeC_2O_4 \longrightarrow 1/4\ Fe + 1/4 + CO + CO_2$$
$$(\Delta H = +141.0\ KJ) \longrightarrow \quad (1)$$

$$FeC_2O_4 \longrightarrow 1/3\ Fe_3O_4 + 4/3\ CO + 2/3\ CO_2$$
$$(\Delta H = +139.5\ KJ) \longrightarrow \quad (2)$$

Figure 1. TG and DTA curves of a) $LiCu_{0.02}Fe_{0.98}PO_4$ and b) $LiSn_{0.02}Fe_{0.98}PO_4$.

Among the two possible paths, it is believed that the decomposition of Fe(II) oxalate will follow reaction 2 in the present study based on the following reasons. Since the prolonged furnace calcination of the precursor mix up to 850° C has not encountered the formation of metallic Fe even in trace levels, as confirmed from XRD results, it is presumed that the thermal decomposition of $Fe(II)C_2O_4$ will follow reaction 2 only. Even in the reaction 2, the formed CO will further be oxidized catalytically to evolve CO_2 [30, 31] and thus the initial weight loss could be attributed to the combined elimination of H_2O and CO_2. Following the decomposition of $Fe_2(C_2O_4)_3$. 6 H_2O salt, an endothermic peak at 175° C in Fig. 1a and an exothermic peak at 189° C in Fig. 1b are observed, which may be correlated to the decomposition of cupric carbonate and stannous chloride respectively. Further, a substantial weight loss of about 6.8% in the temperature range of 175 and 210° C is seen and the same could be ascribed to the combined decomposition of ammonium phosphate monobasic and cupric carbonate/stannous chloride mixture. Similarly, the weight loss recorded around ~415° C may possibly be correlated to the decomposition of lithium carbonate. Further, it is evident from Figs. 1a and b that the DTA curve above 415° C is accompanied by a slow decrease in weight along with an apparent inflection in the TG curve at 516 and 540° C (Figs. 1a-b). Such a slow and continuous decrease in weight of the precursor mix may be attributed to the process of crystallization of newly formed oxide particles. As a result, the total weight loss of ~20% detected at 600° C can be assigned to the monophasic formation of $LiM_XFe_{1-X}PO_4$ (M= Cu, Sn; x= 0.02) compounds.

3.2. Structural results-PXRD studies

The XRD pattern of $LiM_XFe_{1-X}PO_4$/C [M= Cu, Sn]/C composites synthesized via. mechanical ball milling method is shown in Figs. 2a-b. The existence of sharp and well-defined Bragg peaks ensures the presence of phase pure and crystalline products. No peak due to carbon is visible in the PXRD pattern of the resultant $LiM_XFe_{1-X}PO_4$/C composite material (Figs. 1a-b), an indication for the presence of carbon in an amorphous or disordered state [32]. Both the Cu and Sn doped LiFePO4/C composites have exhibited standard orthorhombic olivine type LiFePO4 structure with *Pnma* space group (a =10.35, b = 6.028 and c = 4.703). Particularly, peaks due to Li_3PO_4 and Fe (II, III) pyrophosphate that co-exist normally at temperatures above 700° C has been eliminated in the present study [26]. On the other hand, the existence of 101 (Fig. 2a) plane ($2\theta = 27.7°$) and 202 & 133 (Fig. 2b) planes ($2\theta = 44.7$ and $45.2°$) is due to the presence of Cu and Sn, irrespective of the individual concentration (2%) of the dopants.

Table 1. Physical parameters of $LiCu_{0.02}Fe_{0.98}PO_4$ and $LiSn_{0.02}Fe_{0.98}PO_4$ cathodes

Compound	Lattice Constants			Cell Vol. ($Å^3$)	Cryst. Size (μm)	Stokes strain
	a(Å)	b(Å)	c(Å)			
$LiCu_{0.02}Fe_{0.98}PO_4$	10.35	6.02	4.70	293.4	1.10	1.02
$LiSn_{0.02}Fe_{0.98}PO_4$	10.35	6.02	4.70	293.4	0.93	1.23

The average crystallite size (D) calculated using Scherer's formula and appended in Table 1 was found to remain around 800nm and 1μm, which was further confirmed by the scanning electron micrograph images, obtained for the $LiM_XFe_{1-X}PO_4$ (M= Cu, Sn) samples. In addition, it is understood from the study that the peak broadening in XRD is due to the finite crystallite size only (Table 1) and not due to the instrumental effect or strain, based on the smaller Stoke's strain values calculated using the formula:

$$\varepsilon_{Strain} = \beta/4 \, tan\theta$$

where ε_{Strain} = weighted average strain and β = the integral breadth of a reflection (in radians 2θ) located at 2θ. The calculated strain values are found to be very small (1.02 for $LiCu_{0.02}Fe_{0.98}PO_4$ and 0.96 in case of $LiSn_{0.02}Fe_{0.98}PO_4$) and based on the same, it is further substantiated that the Cu and Sn substituted $LiFePO_4$/C composites have been synthesized with preferred physical properties such as strain free crystal lattice, purity and crystallinity.
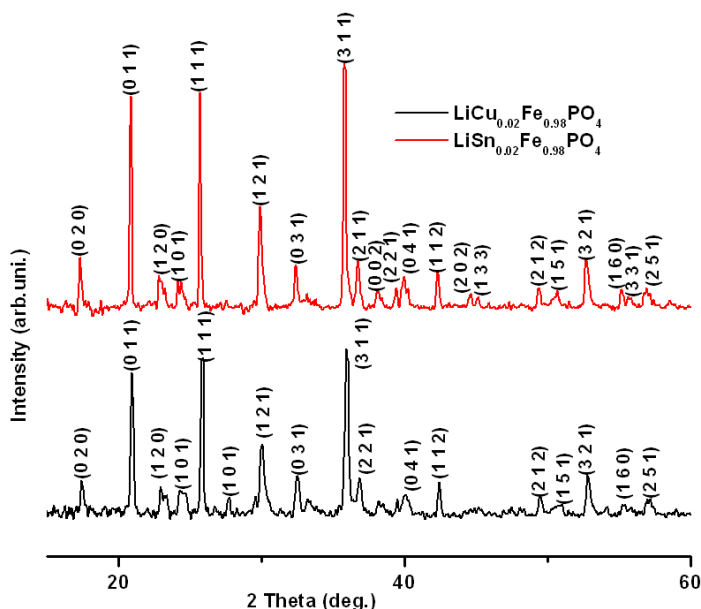

Figure 2. XRD pattern of a) $LiCu_{0.02}Fe_{0.98}PO_4$ and b) $LiSn_{0.02}Fe_{0.98}PO_4.$

3.3. Morphological results-SEM analysis

Surface morphology of $LiM_XFe_{1-X}PO_4$/C [M= Cu, Sn] composites and the nature of the carbon coating have been investigated by Scanning Electron Microscopy. Figs. 3a&b show the scanning electron micrographs (SEM) of $LiCu_{0.02}Fe_{0.98}PO_4$/C and $LiSn_{0.02}Fe_{0.98}PO_4$/C composite powders synthesized from the solid-state ball milling technique. Unlike the literature evidence that supports the formation of irregularly shaped larger particles via. solid-state technique [33], the present study has demonstrated the presence of well-defined spherical particles with finer particle size (Figs 3a-b). Such an observation of absence of particle agglomeration is a preferred property of any electrode material to

exhibit better electrochemical property [34] and thus the present study demonstrates the possibility of synthesizing a variety of doped derivatives of LiFePO$_4$/C cathodes by adopting solid state ball milling technique with duly modified synthesis parameters.
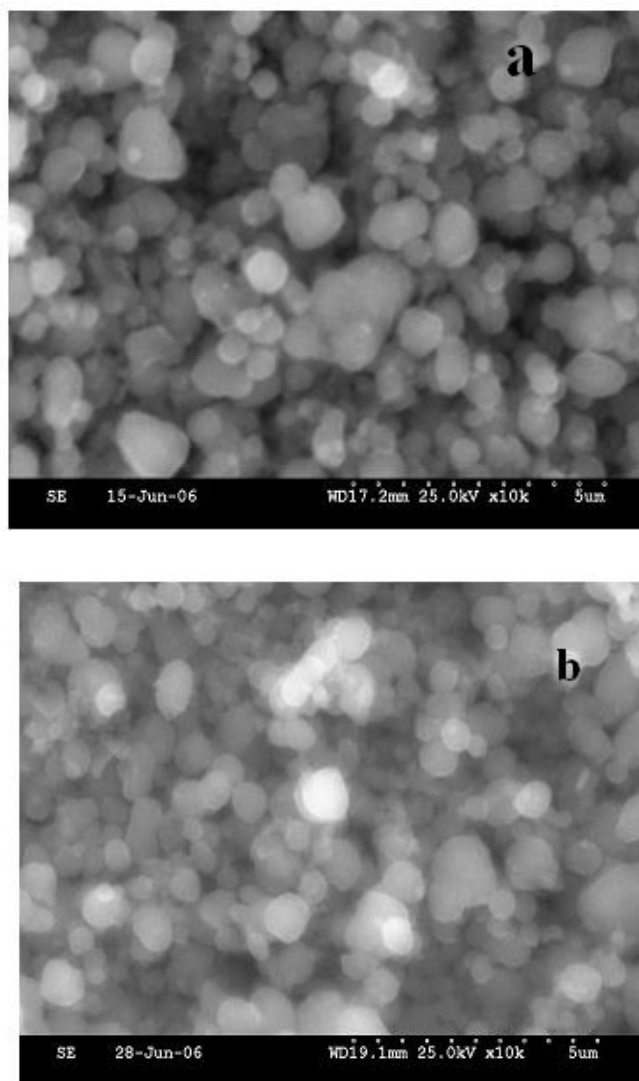

Figure 3. Scanning Electron Micrographs of a) LiCu$_{0.02}$Fe$_{0.98}$PO$_4$ b) LiSn$_{0.02}$Fe$_{0.98}$PO$_4$.

Generally, sintering the precursor above 700° C makes the individual particles to fuse together partially to form large porous agglomerates [33], regardless of the method of grinding / grinding time after the decomposition step. On the other hand, neither an increased particle size nor particle agglomeration was found to be present with the set of chosen category LiM$_X$Fe$_{1-X}$PO$_4$/C materials, which is the highlight of the synthesis approach with systematically adjusted sintering sequence and duly controlled rate of heating. Further, micrographs obtained for both the metal substituted LiFePO$_4$/C powders show similarity in grain structure with an average grain size of ~1μm, which agrees with the average crystallite size calculation deduced from XRD, using Scherer's formula.

3.4. Local cation environment- FTIR study

Basically, vibrational modes that are attributed to the motion of cations with respect to their oxygen neighbors are sensitive to the point group symmetry of the cations in the oxygen/PO_4^{3-} host matrix [35], and hence, the local environment of the cations can be studied by FTIR spectroscopy [36].

The FTIR signatures for the $LiM_XFe_{1-X}PO_4/C$ [M= Cu, Sn] materials are displayed in Fig. 4. The tetrahedral PO_4^{3-} ion has its fundamental vibrational frequencies at 1082, 515, and 980 and 363 cm^{-1} [37], wherein the later pair being normally infrared inactive [38]. Since the orthophosphates show main bands at 1060-1000 cm^{-1} [39] and at 580-520 cm^{-1} [40], the FTIR spectra of $LiM_XFe_{1-X}PO_4/C$ [M= Cu, Sn] obtained in the present study (Fig. 4) has been correlated with those of the reported results of certain other phosphate based compounds. In addition, the entire FTIR spectral pattern of $LiM_XFe_{1-X}PO_4/C$ [M= Cu, Sn] compounds matches well with that of the standard $LiFePO_4$ pattern [41], which is the significance of the study.
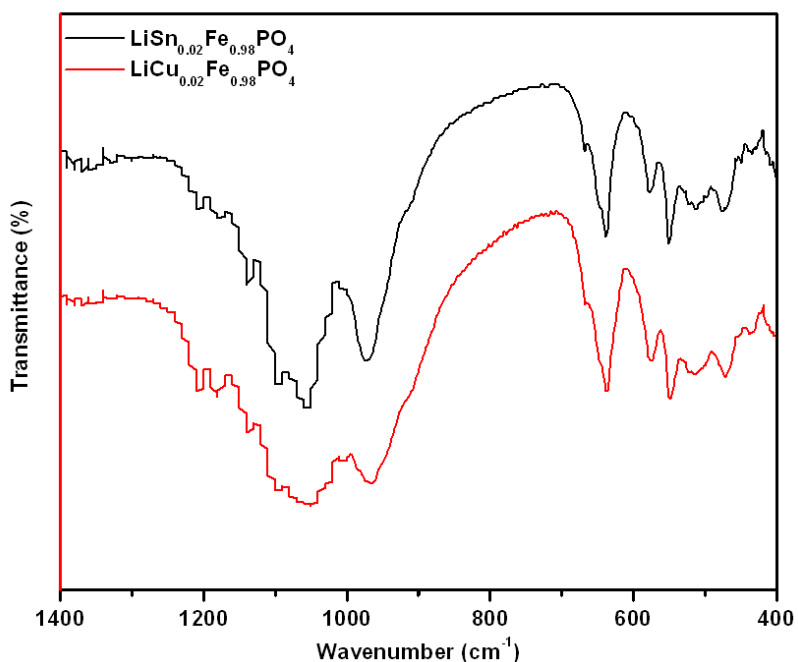

Figure 4. Room temperature FTIR spectrum.

3.5. Electrochemical characterization results

3.5.1. Cyclic voltammetric studies

CV study was performed on Cu/Sn substituted $LiFePO_4$ electrodes with an aim to investigate upon the diffusion kinetics [42] of lithium in the substituted olivine composites. Figs. 5a-b show the cyclic voltammograms of $LiCu_{0.02}Fe_{0.98}PO_4/C$ and $LiSn_{0.02}Fe_{0.98}PO_4/C$ composite at room temperature under a scan rate of 1mV/s between the potential range of 2.5 to 4.5V.

A pair of peaks, consisting of an anodic and a cathodic part has been observed respectively around 3.65V and 3.26V vs. Li /Li$^+$ for both the first and second cycles of LiCu$_{0.02}$Fe$_{0.98}$PO$_4$/C cathode (Fig.4a). Similarly, a set of redox peaks appeared at 3.67 (1st cycle) or 3.97V (2nd cycle) and 3.26V (1st & 2nd cycle) vs. Li/Li$^+$ for LiSn$_{0.02}$Fe$_{0.98}$PO$_4$/C composite (Fig. 5b). The presence of such redox pairs in the said potential range is attributed to the two-phase charge-discharge reaction of Fe^{2+}/Fe^{3+} redox couple [42].
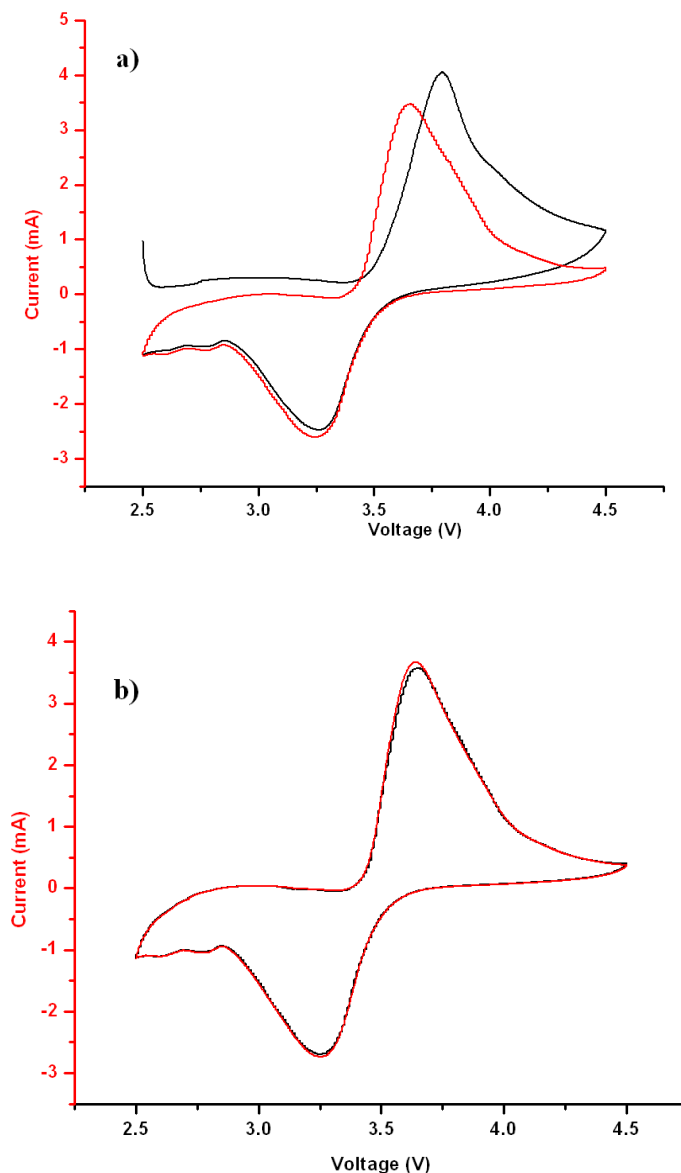

Figure 5. Cyclic voltammogram of a) LiSn$_{0.02}$Fe$_{0.98}$PO$_4$ b) LiCu$_{0.02}$Fe$_{0.98}$PO$_4$.

It is quite interesting to note that among the two cathodes, perfect reproducibility of anodic (3.65V) and cathodic (3.26V) peaks exactly in their respective positions observed upon successive cycles (Fig. 5a) arbitrates the augmentation of excellent reversibility of insertion / extraction of Li in the LiCu$_{0.02}$Fe$_{0.98}$PO$_4$/C composite electrode. Similarly, the difference between the potential separation

of anodic and cathodic peaks (0.12V) corresponding to $LiSn_{0.02}Fe_{0.98}PO_4$/C seems to be meager (<0.2V). Such an electrochemical behavior is an indication for good electrode or diffusion kinetics, especially while considering the electrochemical process that involves the diffusion of lithium ions in a solid phase and electron jumping across a poorly or fairly conducting compound [43].

Further, the CV profile of the first cycle in $LiSn_{0.02}Fe_{0.98}PO_4$ (Fig. 5b) corresponds to an obvious polarization with a potential separation of 0.53V between anode and cathode peaks, whereas the potential separation encountered in the second cycle was only 0.40V. This phenomenon is ascribed to the morphology changes that possibly occur during the first formation cycle [44]. Based on this, either the generation of a mosaic structure [45] or the breakdown of crystal aggregates [45] could be suggested as possible mechanisms involved in the electrochemical cycling process of $LiSn_{0.02}Fe_{0.98}PO_4$ cathode. Moreover it is worth mentioning here that Padhi etal., [2] have reported that the electrochemical lithium insertion/extraction reactions of $Li_3Fe_2(PO_4)_3$, $LiFeP_2O_7$ and $Fe_4(P_2O_7)_3$ occur at 2.8, 2.9, and 3.1V vs. Li/Li^+ respectively. However, no such peaks corresponding to lithium insertion/extraction reactions of mentioned category undesirable iron phosphates were observed, (Figs. 5a-b) thereby confirms the phase purity of the synthesized metal substituted $LiFePO_4$/C composites of the present study [8]. Thus, the results obtained from XRD related to the phase purity of synthesized $LiCu_{0.02}Fe_{0.98}PO_4$/C and $LiSn_{0.02}Fe_{0.98}PO_4$/C compounds could be substantiated further through CV studies also.

3.5.2. Charge discharge studies

The capacity vs. cycleability behavior of metal substituted $LiFePO_4$/C composite cathodes examined at room temperature under a constant current drain of 0.5mA and at a potential window of 2.5 - 4.2V is shown in Figs. 6&7.
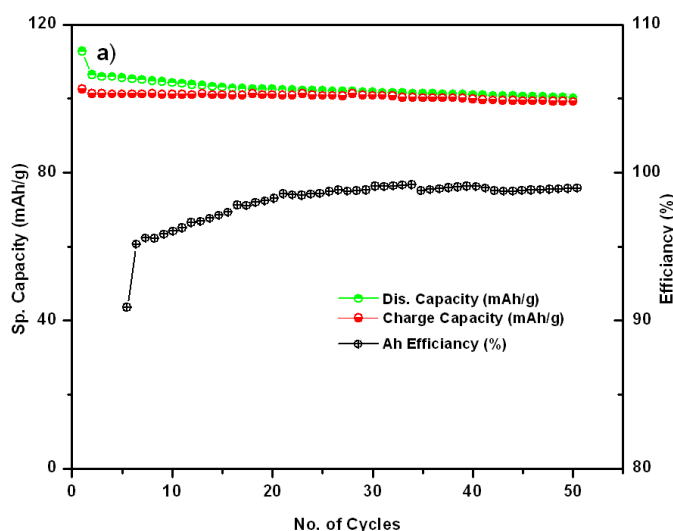

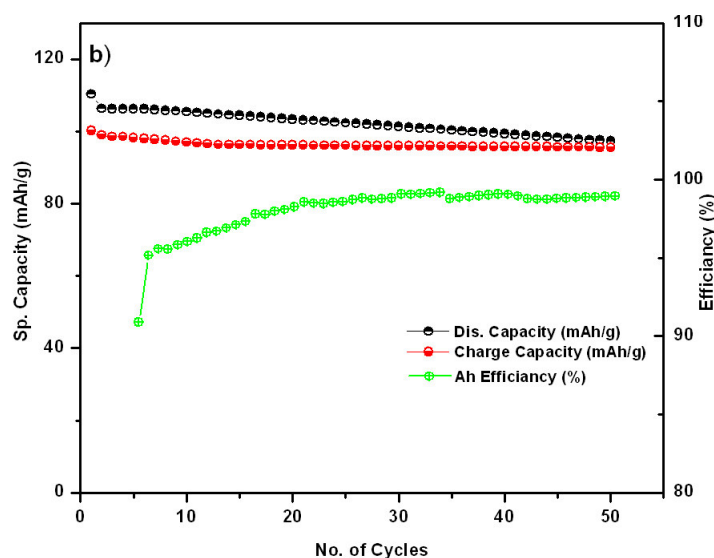**Figure 6.** Capacity *vs.* cycle number of $LiCu_{0.02}Fe_{0.98}PO_4$.

Figure 7. Capacity *vs.* cycle number of $LiSn_{0.02}Fe_{0.98}PO_4$.

It is well known that the discharge capacity of $LiFePO_4$/C composite decreases significantly with an increase in discharge current because of its poor electronic conductivity [8]. On the contrary, reasonably high specific capacity values of ~112 and 110 mAh/g have been exhibited (Table 2) by the $LiCu_{0.02}Fe_{0.98}PO_4$/C and $LiSn_{0.02}Fe_{0.98}PO_4$/C composite cathodes, which are relatively higher than the specific capacity of native $LiFePO_4$, when discharged at the rate of 0.5 mA. In addition to the enhanced initial capacity, the synthesized cathodes have demonstrated a better reversibility and steady state capacity around 105 and 100 mAh/g corresponding to $LiCu_{0.02}Fe_{0.98}PO_4$/C and $LiSn_{0.02}Fe_{0.98}PO_4$/C electrodes. In particular, $LiCu_{0.02}Fe_{0.98}PO_4$/C has exhibited an excellent reversible capacity characteristics (Q_{dc}/Q_c), such as improved capacity retention behavior (>90%) and excellent coulumbic efficiency values (96-98%). Similarly, $LiSn_{0.02}Fe_{0.98}PO_4$/C cathode has shown fairly stable charge discharge capacity behavior (in the range of 100-110 mAh/g) up to 50 cycles, with progressively enhanced Ah efficiency values (90-96%), as evidenced in Table 2.

Table 2. Electrochemical parameters of $LiCu_{0.02}Fe_{0.98}PO_4$ and $LiSn_{0.02}Fe_{0.98}PO_4$ cathodes

Compound	Discharge capacity Qd (mAh/g) vs. Cycles life						Charge capacity Qc (mAh/g) vs. Cycles life						Efficiancy (%)	
	1	10	20	30	40	50	1	10	20	30	40	50	1	50
$LiCu_{0.02}Fe_{0.98}PO_4$	112	110	108	107	106	105	107	105	104	104	103	10295	97	
$LiSn_{0.02}Fe_{0.98}PO_4$	110	109	107	105	102	101	101	99	98	97	96	96	91	95
$LiFePO_4$	105	-	100	-	98	97	95	-	92	-	91	91	90	94

Hence, it is understood from the present study that the effect of transition metal (Cu) is found to enhance the realizable specific capacity values (>100mAh/g) even at 0.5mA discharge rates. Similarly, the doped non-transition metal (Sn) is found to minimize the capacity fade significantly upon cycling, especially at the said discharge rate.

4. CONCLUSIONS

$LiCu_{0.02}Fe_{0.98}PO_4/C$ and $LiSn_{0.02}Fe_{0.98}PO_4/C$ cathodes were prepared by a simple solid state ball milling technique with duly modified synthetic conditions and carefully monitored sintering sequence. As a result, phase pure and crystalline powders of $LiCu_{0.02}Fe_{0.98}PO_4/C$ and $LiSn_{0.02}Fe_{0.98}PO_4/C$ cathodes with preferred physical characteristics such as sub-micron particle size (<1μm) and uniformly distributed spherical grains with proper grain boundaries were obtained at 750° C. Further, the synthesized $LiCu_{0.02}Fe_{0.98}PO_4/C$ & $LiSn_{0.02}Fe_{0.98}PO_4/C$ cathodes have exhibited apparent specific capacity values (>100mAh/g) with excellent reversibility and Ah efficiency values under the influence of 0.5mAdischarge rate. The enhanced reversible capacity values (~105 mAh/g) and minimized capacity fade values upon extended cycling (<5%) are realized as the effect of Cu and Sn dopants respectively upon $LiFePO_4$ matrix.

References

1. A. K. Padhi, K. S. Nanjundaswamy, J. B. Goodenough, *J. Electrochem. Soc.,* 144 (1997) 1188.
2. A. K. Padhi, K. S. Nanjundaswamy, C. Masquelier, S. Okada, and J. B. Goodenough, *J. Electrochem. Soc.,* 144 (1997) 1609.
3. K. Amine, H. Yasuda, and M. Yamachi, *Electrochem. Solid-State Lett.,* 3 (2000) 178.
4. J. J. Papike and M. Camaron, *Rev. Geophys. Space phys.,* 14 (1976) 37.
5. J. –M. Tarascon and M. Armand, *Nature,* (London) 414 (2001) 359.
6. A. Yamada, S. C. Chung, and K. Hinokuma, *J. Electrochem. Soc.,* 148 (2001) A224.
7. A. S. Andersson, J. O. Thomas, B. Kalska, and L. Haggstroem, *Electrochem. Solid-State Lett.,* 3 (2000) 66.
8. Y. Iriyama, M. Yokoyama, C. Yada, S. K. Jeong, I. Yamada, T. Abe, M. Inaba, Z. Ogumi, *Electrochem. Solid-State Lett.,* 7 (2004) A 340.
9. A. S. Anderson, , b. Kalska, L. Haggstrom, and J. O. Thomas, *Solid State Ionics,* 130 (2000) 41.
10. A. Yamada, Y. Kudo, and, K. Y. Liu, *J. Electrochem. Soc.,* 148 (2001) A1153.
11. M. C. Tucker, M. M. Doeff, T. J. Richardson, R. Finones, J. A. Reimer, E. J. Cairnes, *Electrochem. Solid-State Lett.*, 5 (2002) A 95.
12. C. M. Burba, and R. Frech, *J. Electrochem. Soc.,* 151 (2004) A1032.
13. N. Ravet, J. B. Goodenough, S. Besner, M. Simoneau, P. Hovington, and M.Armand, Abstract 127, The Electrochemical society meeting abstracts, Vol. 99-2Honolulu, Hi, Oct 17-22, 1999.
14. P. P. Prosini, D. Zane, M. Pasquali, *Electrochim. Acta,* 46 (2001) 3517.
15. S. Y. Chung, J. T. Bloking, and Y. M. Chiang, *Nat. Mater.,* 1 (2003) 123.

16. J. Barker, M. Y. Saidi and J. L. Swoyer, *Electrochem. Solid- State Lett*., 6 (2003)A53.
17. H. Liu, Q. Cao, L.J. Fu, C. Li, Y.P. Wu , H.Q. Wu, *Electrochem. Commun.,* 8 (2006) 1553.
18. F. Sauvage, E. Baudrin, M. Morerette and J. M. Raeascon *Electrochem. Solid- State Lett.,* 7 (2004) A 15.
19. Z. Chen and R. Dhan, *J. Electrochem. Soc*., 149 (2002) 1184.
20. R. Domniko, M. Geberscek, J. Drofenik, M. Bele, S. Pejovnik, and J. Jamnik, *J. Power Sources,* 119-121 (2003) 770.
21. M. M. Doeff, Y. Hu, F. Mclarnon, and R. Kostecki, *Electrochem. Solid-State Lett.,* 6 (2003) A207.
22. J. Yang and J. J. Xu, *Electrochem. Solid-State Lett.,* 7 (2004) A515.
23. K. S. Park, J. T. Son, H. T. Chung, S. J. Kim, C. H. Lee, H. G. Kim*, Electrochem. Commun.,* 5 (2003) 839.
24. S. T. Myung, S. Komaba, N. Hirosaki, H. Yoshiro, N. Kumogai, *Electrochim. Acta* 49 (2004) 4213.
25. M. Higuchi, K. Katayama, Y. Azuma, M. Yukawa, M. Suhara, *J.Power Sources*, 119-121 (2003) 259.
26. N. Kalaiselvi, C. H. Doh, C. W. Park, S. I. Moon, M. S. Yun, *Electrochem. Commun*., 6 (2004) 110.
27. N. Jayaprakash and N. Kalaiselvi, *Electrochem. Commun.*, 9 (2007) 620.
28. M. Hermanek, R. Zboril, M. Mashlan, L. Machala , O. Schneeweiss, *J. Mat Chemistry.,* 16 (2006)
29. CRC Handbook Chem. Phys., 70th edn. (1989±1990).
30. D. Dollimore, *Thermochim. Acta,* 117 (1987) 331.
31. D. Dollimore, *J. Therm. Anal.,* 11 (1977) 187.
32. X. Z. Liao, Z. F. Ma, L. Wang, X. Ming, Y. Jiang, and Y. S. He, *Electrochem. Solid- State Lett.,* 7A (2004) 522.
33. Yaoqin Hu, Marca M. Doeff, Robert Kostecki and Rita Finones *J. Electrochem. Soc.,* 151A (2004) 1279.
34. N. Jayaprakash, K. Sathiyanarayanan and N. Kalaiselvi, *Electrochim. Acta,* 52 (2007) 2453.
35. C. J. Rougier, G. A. Nazri, C. Julian, *Mater. Res. Soc. Symp. Proc*, 453 (1997) 647.
36. A. Rouier, G. A. Nazri, C. Julian, *Ionics*, 3 (1997) 170.
37. Corbridge. D. E. C, *J. Appl. Chem*,. 6 (1956) 456.
38. Hersberg. G., Infra-Red and Raman Spectra pf Polyatomic Molecules., 1945 (New York: Van Nostrand).
39. Miller. F. A., and Wilkins. C. H., *Analyt. Chem*., 24 (1952)1253.
40. Duval. C., and Lacompte. J., C. R. Acad. Sci., Paris 1954; 239:249.
41. Inorganic Library of FTIR Spectra- Minerals., ©NICODOM, Volume 1, 1998.
42. M. Takahashi, Shin-ichi Tobishima, K. Takei, Y. Sakurai, *Solid State Ionics,* 148 (2002) 283.
43. A. Croce, A. D. Epifanio, J. Hassoun, A. Deptula, T. Olczac and B. Scrosati, *Electrochem. Solid-State Lett.,* 5 (2002) A 47.
44. X. Z. Liao, Z. F. Ma, L. Wang, X. M. Zhang, Y. Jiang and Y. S. He., *Electrochem. Solid-State Lett.,* 7 (2004) A 522.
45. A. S. Anderesson, and J. O. Thomas, *J. Power Sources,* 97-98 (2001) 498.